The Dartmouth Stellar Evolution Database

Aaron Dotter and Brian Chaboyer

Department of Physics and Astronomy, Dartmouth College, 6127 Wilder Laboratory, Hanover, NH 03755

Darko Jevremović[1]

Astronomical Observatory, Volgina 7, 11160 Belgrade, Serbia

Veselin Kostov and E. Baron[2]

Homer L. Dodge Department of Physics and Astronomy, University of Oklahoma, 440 West Brooks, Room 100, Norman, OK 73019-2061

Jason W. Ferguson

Physics Department, Wichita State University, Wichita, KS 67260-0032

ABSTRACT

The ever–expanding depth and quality of photometric and spectroscopic observations of stellar populations increase the need for theoretical models in regions of age–composition parameter space that are largely unexplored at present. Stellar evolution models that employ the most advanced physics and cover a wide range of compositions are needed to extract the most information from current observations of both resolved and unresolved stellar populations. The Dartmouth Stellar Evolution Database is a collection of stellar evolution tracks and isochrones that spans a range of [Fe/H] from –2.5 to +0.5, [α/Fe] from –0.2 to +0.8 (for [Fe/H] $\leq$0) or +0.2 (for [Fe/H] >0), and initial He mass fractions from Y=0.245 to 0.40. Stellar evolution tracks were computed for masses between 0.1

[1]Homer L. Dodge Department of Physics and Astronomy, University of Oklahoma, 440 West Brooks, Room 100, Norman, OK 73019-2061

[2]Computational Research Division, Lawrence Berkeley National Laboratory, MS 50F-1650, 1 Cyclotron Rd, Berkeley, CA 94720

and 4 $M_\odot$ allowing isochrones to be generated for ages as young as 250 Myr. For the range in masses where the core He flash occurs, separate He-burning tracks were computed starting from the zero age horizontal branch. The tracks and isochrones have been transformed to the observational plane in a variety of photometric systems including standard UBV(RI)$_C$, Strömgren uvby, the Sloan Digital Sky Survey ugriz, the Two Micron All Sky Survey JHK$_s$, and Hubble Space Telescope ACS-WFC and WFPC2. The Dartmouth Stellar Evolution Database is accessible through a website[1] where all tracks, isochrones, and additional files can be downloaded.

Subject headings: globular clusters: general — open clusters: general — stars: evolution

1. Introduction

Recent photometric surveys such as the ACS Survey of Galactic Globular Clusters (Sarajedini et al. 2007) have substantially increased the quality and volume of data available for the Galactic globular cluster system. Despite the fact that this survey focused on metal poor stellar populations it was found that there was a need for stellar evolution models with [Fe/H] >0 (Siegel et al. 2007). Many other photometric surveys such as the Two Micron All Sky Survey[2] (2MASS) and the Sloan Digital Sky Survey[3] (SDSS) and extensions such as SEGUE[4] underscore the need for stellar evolution libraries that span a wide range of compositions and photometric systems.

Dotter et al. (2007) introduced a set of stellar evolution tracks, isochrones, and computer programs to accompany the ACS Survey of Galactic Globular Clusters. The set includes tracks with masses between 0.1 and 1.8 $M_\odot$, isochrones with ages ranging from 2 to 15 Gyr, [Fe/H] from –2.5 to 0 with a variety of options in [α/Fe] and initial He content (Y$_{init}$). In this paper, that set of models is expanded to include: (i) tracks and isochrones with [Fe/H]= +0.15, +0.3, and +0.5; (ii) higher mass tracks and isochrones with ages as low as 250 Myr for all compositions; (iii) a wider selection of photometric systems; and (iv) a web interface to

---

[1]http://stellar.dartmouth.edu/~models/

[2]http://pegasus.phast.umass.edu/

[3]http://www.sdss.org/

[4]http://segue.uchicago.edu/

three of the computer programs so that visitors can easily generate specific models without downloading the entire database and running the programs locally.

Collectively, these tracks, isochrones, and supporting computer programs constitute the Dartmouth Stellar Evolution Database. The stellar evolution code used to generate these models is reviewed in §2. Details of the compositions and model grids are outlined in §3 and the color–T_{eff} transformations in §4. In §5, the isochrones are compared to those of comparable isochrone libraries and photometry of Galactic open clusters and one globular cluster. The results are summarized and discussed in §6.

2.   The Dartmouth Stellar Evolution Program

The Dartmouth Stellar Evolution Program (DSEP) has been described previously by Bjork & Chaboyer (2006) and Dotter et al. (2007). The following is a brief description of the physics employed by DSEP.

Partially inhibited atomic diffusion and gravitational settling of both He (Y) and metals (Z) are included as described by Chaboyer et al. (2001). Diffusion is calculated based on the formalism of Thoul et al. (1994) but inhibited in the outer 0.01 $M_{\odot}$ where the diffusion coefficients are set to zero in the outermost 0.005 $M_{\odot}$ and ramped from zero to full diffusion in the inner 0.05 $M_{\odot}$. This method produces results that are consistent with recent observations of diffusion in NGC 6397 (Korn et al. 2006).

DSEP uses high temperature opacities from OPAL (Iglesias & Rogers 1996) and low temperature opacities based on Ferguson et al. (2005). The OPAL tables were obtained for each of the different [α/Fe] mixtures from the OPAL web interface [5] and the low temperature tables were calculated by one of us (Ferguson). The low temperature opacity tables have been made available via the World Wide Web[6]. Conductive opacities are taken from Hubbard & Lampe (1969).

The basic equation of state (EOS) in DSEP is a general ideal gas EOS with the Debye-Hückel correction (Chaboyer & Kim 1995) and is used for tracks with M $\geq$ 0.8$M_{\odot}$. For lower mass tracks (M< 0.8$M_{\odot}$), the FreeEOS equation of state (Irwin 2004) is used in the EOS4 configuration.

DSEP treats convection with the standard mixing length theory and a solar-calibrated

---

[5]http://www-phys.llnl.gov/Research/OPAL/

[6]http://webs.wichita.edu/physics/opacity/

mixing length, α_{ML}=1.938. The models include convective core overshoot according to the scheme developed by Demarque et al. (2004). The underlying idea is that the amount of overshoot grows with the size of the convective core. The amount of core overshoot is parametrized as a multiple of the pressure scale height (λ_P) and is a function of stellar mass and composition. The minimum stellar mass receives 0.05 λ_P of overshooting, models with masses greater than the minimum by 0.1 $M_\odot$ receive 0.1 λ_P of overshooting, and models with masses greater than or equal to the minimum plus 0.2 $M_\odot$ receive 0.2 λ_P of overshooting. For details on the minimum mass as a function of composition see Table 1. Convective envelope undershooting is not considered in these models.

The surface boundary condition (BC) was derived from a grid of PHOENIX model atmospheres (Hauschildt et al. 1999a,b) covering T_{eff}=2,000 to 10,000 K and log g=–0.5 to 5.5. The solar abundance scale used in these calculations was that of Grevesse & Sauval (1998, hereafter GS98). PHOENIX model atmosphere grids were computed for the full range [Fe/H]=–2.5 to +0.5 and [α/Fe]=–0.2 to +0.8 covered by the stellar evolution calculations. A small number of model atmospheres with enhanced He were also computed to gauge the importance of enhanced He to the physical structure and the spectrum. The gas pressure (and thus the surface BC) experiences a small change with enhanced He and this is accounted for in the surface BC.

Castelli & Kurucz (2003) atmospheres were used for $T_{\text{eff}} > 10,000$ K; Castelli & Kurucz (2003) models were computed only for [α/Fe]=0 and +0.4. Stellar evolution models with [α/Fe] $\leq$ +0.2 made use of surface BC derived from [α/Fe] = 0 model atmospheres for $T_{\text{eff}} > 10,000$ K. For stellar evolution models with [α/Fe] $\geq$ +0.4 the [α/Fe] = +0.4 boundary conditions were used for $T_{\text{eff}} > 10,000$ K. The transition between the PHOENIX and Castelli & Kurucz (2003) were always smooth regardless of the composition. The smooth transition is due to the stellar evolution models being relatively insensitive to the surface BC at higher T_{eff} coupled with the reduced sensitivity of the model atmospheres to abundance variations in the transitional T_{eff}.

The surface BC was fit at the point in the atmospheric structure where $T=T_{\text{eff}}$ for a given model. The gas pressure was extracted at $T=T_{\text{eff}}$ and added to the radiation pressure to satisfy the surface BC. Vandenberg et al. (2007) found that, at least in the vicinity of 1 $M_\odot$, the choice of model atmosphere boundary condition fitting point (either at $T=T_{\text{eff}}$ or at an optical depth of τ=100) has little influence on the resulting evolution.

The PHOENIX model atmosphere code employs its own set of physics that is not identical to the physics used in DSEP, though there is some overlap. In particular, the low temperature opacities of Ferguson et al. (2005) are calculated with PHOENIX and this implies a level of consistency between the two codes. PHOENIX employs a standard mixing length theory of

convection with mixing length $\alpha_{MLT} = 2.0$ (whereas DSEP uses $\alpha_{MLT} = 1.938$). Perhaps the largest difference between PHOENIX and DSEP in terms of stellar structure is the EOS: PHOENIX uses an ideal EOS that includes the contributions of a large number of elements and molecules while FreeEOS (used by DSEP) includes several non-ideal effects but accounts for fewer elements and only molecules involving combinations of H and He.

The nuclear reaction rates are taken from Adelberger et al. (1998) for most reactions. The exceptions are the $^{14}N(p,\gamma)^{15}O$ reaction (Imbriani et al. 2004), the triple-α reaction from the NACRE compilation (Angulo et al. 1999), and the $^{12}C(\alpha,\gamma)^{16}O$ reaction (Kunz et al. 2002). Neutrino cooling rates were taken from Haft et al. (1994).

3. Model Grids and Supporting Programs

Stellar evolution models were computed using one of six different heavy element mixtures with the distinguishing characteristic of each mixture being the level of α-element enhancement. Opacities were generated for each of $[\alpha/Fe]$= –0.2, 0, 0.2, 0.4, 0.6, and 0.8. The heavy element mass fractions of these mixtures are given in Table 2. The mixtures were calculated starting with the solar mixture of GS98 by adding the value of $[\alpha/Fe]$ to the log(N+12) abundance of each of the following α-elements: O, Ne, Mg, Si, S, Ca, and Ti; the abundance of Ar was not altered from its GS98 value in any of the mixtures.

Overall, models were computed for 67 different X,Z pairs; the initial compositions are listed in Table 3. For $[Fe/H] > 0$ the maximum level of α-enhancement was chosen to be $[\alpha/Fe]$=+0.2 in order to keep the total Z value below 0.1 since the opacity tables do not extend above Z=0.1. The model atmosphere grid included only provided scaled-solar ($[\alpha/Fe]$=0) models at $[Fe/H]$=+0.15. The He content of the models begins with Y=0.245 at $[Fe/H]$ = –2.5, consistent with Spergel et al. (2003), and a He enrichment relation of $\Delta Y/\Delta Z$=1.54. For $[Fe/H] \leq 0$, additional models were computed with Y=0.33 and 0.40 (see Table 3).

Stellar evolution tracks were computed for stellar masses ranging from 0.1 to 4 $M_\odot$ in increments of 0.05 $M_\odot$ (between 0.1 and 1.8 $M_\odot$), 0.1 $M_\odot$ (between 1.8 and 3 $M_\odot$), and 0.2 $M_\odot$ (between 3 and 4 $M_\odot$). The tracks cover the evolution of the models from the fully convective pre-main sequence (pre-MS) to either the core He flash for M $\lesssim$ 2 $M_\odot$ or either 100 Gyr or the top of the white dwarf cooling curve (whichever came first) for M $\lesssim$ 0.5 $M_\odot$. For models that experience the core He flash, separate He burning tracks were evolved from the Zero Age Horizontal Branch (ZAHB) using the surface compositions and He core masses listed in Tables 4 and 5, respectively. For models that either transition smoothly to core

He burning (M $\gtrsim$ 2 M$_\odot$) or were evolved from the ZAHB, the He–burning evolution was followed until the onset of thermal pulsations on the asymptotic giant branch (AGB).

Isochrones were generated from these tracks with ages from 250 Myr to 15 Gyr in increments of: 50 Myr between 250 Myr and 1 Gyr, 250 Myr between 1 and 5 Gyr, and 500 Myr between 5 and 15 Gyr. The isochrones extend from the lower MS to the tip of the red giant branch (RGB) or, for ages where the tracks permit it (MS mass above ∼2 M$_\odot$), at or near the onset of the thermal pulsations on the AGB [7]. The low mass limit of the isochrones depends on the age: the isochrones only include masses for which the models have reached the MS. The lowest mass stars considered in this paper (0.1 M$_\odot$) may require ∼1 Gyr before reaching the MS and therefore will not be present in isochrones for younger ages. For example, the [Fe/H]=0 isochrones have the following minimum masses (M$_\odot$): 0.43 at 250 Myr, 0.32 at 500 Myr, 0.22 at 750 Myr, and 0.11 at 1 Gyr. Evolutionary tracks are also provided and these include the pre-MS evolution for all masses.

All tracks and isochrones were transformed to the color-magnitude diagram (CMD) using each of the color-T$_{\text{eff}}$ transformations described in §4. The track files consist of lines indicating age, log T$_{\text{eff}}$, log g, log L/L$_\odot$, followed by the absolute magnitude in each of the filters for a given photometric system. A theoretical track file is also available, this file contains age, log T$_{\text{eff}}$, log g, log L/L$_\odot$, log R/R$_\odot$, core He mass fraction (Y$_{core}$), core Z mass fraction (Z$_{core}$), the surface Z/X ratio, H–burning luminosity (L$_\odot$), He–burning luminosity (L$_\odot$), He core mass, and C/O core mass. The isochrones list stellar mass, log T$_{\text{eff}}$, log g, log L/L$_\odot$, and absolute magnitude in each of the filters for a given photometric system.

The collection of Fortran 77 programs introduced by Dotter et al. (2007) have been updated to deal with the expanded compositions and photometric systems presented in this paper but are otherwise largely unchanged. See the appendices of Dotter et al. (2007) for a detailed description of these programs and their output.

4. Color-T$_{\text{eff}}$ Transformations

Synthetic color-T$_{\text{eff}}$ transformations were derived from the PHOENIX model atmosphere grid (also used to generate surface boundary conditions in the stellar evolution calculations)

---

[7]Due to the mass spacing of the stellar evolution tracks and the interpolation used in isochrone generation, the isochrones that include the AGB do not always terminate at the 'tip' of the AGB. In this case, it is recommended to examine the stellar evolution tracks if the brightness of the stars at the onset of the TP-AGB stage is of interest. This applies only to iscohrones with ages below 1 Gyr. Isochrones with ages above 1 Gyr that include only the RGB provide reasonably accurate estimates of the RGB tip as a function of age.

for $T_{eff} < 10,000$ K and for all [Fe/H] and [α/Fe] combinations. The PHOENIX grid was supplemented by Castelli & Kurucz (2003) models for higher T_{eff}. In order to insure a smooth transition, the Castelli & Kurucz (2003) colors were adjusted to line up with the PHOENIX colors at 10,000 K and the two sets of tables were ramped between PHOENIX and Castelli & Kurucz (2003) in the temperature range of 9,000 K to 10,000 K.

As mentioned in §2, the PHOENIX model atmospheres used to generate synthetic color–T_{eff} transformations were computed for each of the [Fe/H], [α/Fe] pairs but not for all of the enhanced Y values. The influence of enhanced He on broad-band synthetic photometry is negligible for the temperatures considered here, as discussed briefly by Dotter et al. (2007) and in more detail by Girardi et al. (2007).

The Castelli & Kurucz (2003) model atmospheres were only computed for [α/Fe]=0 and +0.4. In constructing the color transformations the same approach was used as described in §2 for the surface BC. For evolutionary tracks and isochrones with [α/Fe] $\leq$ +0.2, colors based on Castelli & Kurucz (2003) synthetic spectra with [α/Fe] $= 0$ were applied and for tracks and isochrones with [α/Fe] $\geq$ +0.4, colors based on Castelli & Kurucz (2003) synthetic spectra with [α/Fe] $= +0.4$ were applied. While this is not an ideal situation, the influence of α-enhancement, or indeed of total Z, on broad-band synthetic colors is small for $T_{eff} \gtrsim$ 5,000 K. The only exceptions are in the bluest bands (equivalent to U) and at $T_{eff} \gtrsim 35,000$ K. Bands equivalent to U are the most uncertain in terms of the synthetic photometry and very few of the evolutionary tracks (only the lowest mass, metal poor He-burning tracks) presented in this paper extend beyond $T_{eff} = 35,000$ K.

The synthetic colors have been tested and perform well in bandpasses equivalent to V or redder (with central wavelengths longer than $\sim$ 5000 Å) but the blue and ultraviolet bands (with central wavelengths shorter than $\sim$ 5000 Å) suffer from inaccuracy of the synthetic fluxes at shorter wavelengths. In cases where analysis in the bluer bands is important, empirical color transformations are strongly recommended.

Cassisi et al. (2004) explored the dependence of broadband synthetic colors on [α/Fe] for [α/Fe]=0 and +0.4. Their findings indicate that U–B and B–V are the colors most strongly effected by α-enhancement and that the influence of α-enhancement on broadband colors increases with increasing metallicity and decreasing T_{eff}. The color transformations derived from the PHOENIX model atmosphere grid have a greater span of T_{eff} and [α/Fe], including [α/Fe] $= -0.2$ for the first time, and better resolution (0.2 dex) in [α/Fe]. The comparisons performed with the PHOENIX synthetic colors qualitatively agree with the findings of Cassisi et al. (2004) though it is important to recognize that Cassisi et al. (2004) compared colors at constant Z while in this paper comparisons are made at constant [Fe/H]. Hence an increase in [α/Fe] represents an increase in total Z and thus one expects the colors to

become redder with increasing $[\alpha/\text{Fe}]$ as a general rule.

Figure 1 displays the changes to CMD morphology based solely on the level of α-enhancement at $[\text{Fe/H}]=0$ using a 10 Gyr scaled-solar isochrone. The figure shows $[\alpha/\text{Fe}] = 0$, $+0.4$, and $+0.8$ colors. The comparisons were assembled using a scaled-solar isochrone in order to demonstrate the effect of α-enhancement on the colors only. Two colors, V–I and J–K_s are shown in Figure 1. The figure shows that V–I increases with $[\alpha/\text{Fe}]$ and while the difference is small near the MSTO, it grows as T_{eff} decreases, becoming largest near $M_V = 10$. The situation in J–K_s is reversed: the highest level of $[\alpha/\text{Fe}]$ produces the bluest J–K_s color while the lowest level produces the reddest color. The J–K_s result is, at first glance, counter-intuitive. However, the J band is particularly sensitive to absorption from water and, in the presence of enhanced oxygen (from $[\alpha/\text{Fe}]$), substantially more water is able to form. This pushes flux away from the J band and causes the J–K_s color to become bluer with increasing $[\alpha/\text{Fe}]$.

As reported by Cassisi et al. (2004), the color differences due to variations in $[\alpha/\text{Fe}]$ decrease as total metallicity decreases. However, isochrones presented in this paper suggest that the separation along the lower MS in J–K_s remains noticeable even at $[\text{Fe/H}]=-2$ and this feature may prove a useful diagnostic for near infrared studies of metal poor systems of sufficient depth to see the lower MS.

The remainder of this section give a brief description of the photometric systems into which the stellar evolution tracks and isochrones have been transformed.

4.1. Johnson–Cousins UBVRI and the Two Micron All Sky Survey

Bessell (1990) defined filter transmission curves for the Johnson–Cousins UBV(RI)_C photometric system. These filter curves were combined with 2MASS JHK_s filters from Cohen et al. (2003) to create a set of isochrones suitable for use with ground–based photometry from the ultraviolet to the near infrared. The UBVRI magnitudes were calibrated to Vega by following Appendix A of Bessell et al. (1998). The 2MASS magnitudes were calibrated by setting the magnitudes of Vega to zero in each filter (Cohen et al. 2003).

4.2. The Hubble Space Telescope

Bedin et al. (2005) defined a method for generating synthetic photometry based on the detailed filter transmission curves for the Hubble Space Telescope (HST) Advanced Camera for Surveys (ACS) and Wide Field Planetary Camera 2 (WFPC2) from Sirianni et al. (2005).
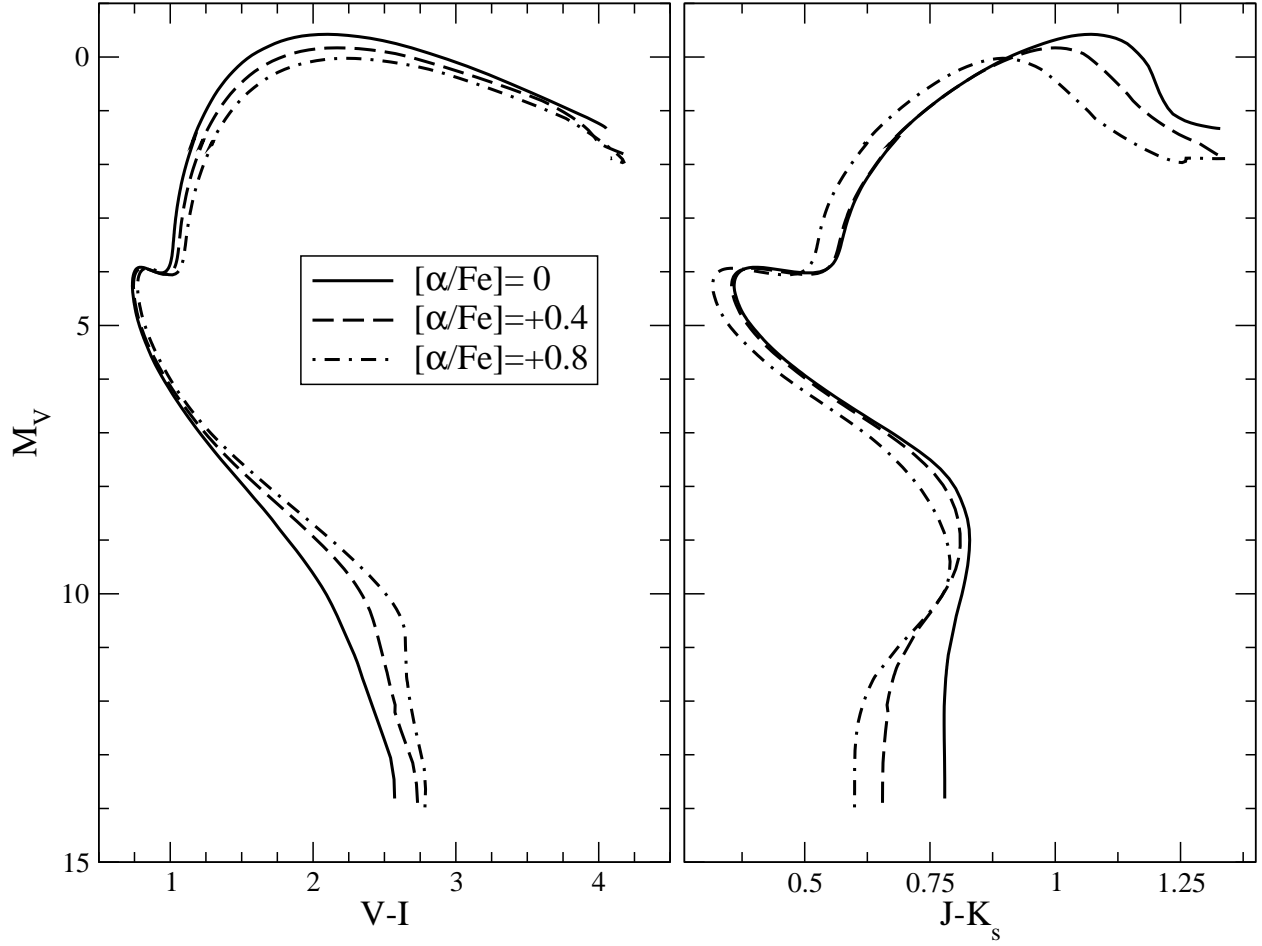
Fig. 1.— The influence of α-enhancement on broadband V–I and J–K$_s$ colors at [Fe/H] = 0. The underlying isochrones shown are all scaled-solar composition with [Fe/H] = 0 at 10 Gyr. Only the color transformations include α-enhancement. See the text for a discussion of the trends shown in the figure.

The synthetic photometry presented here are all on the Vegamag system. The following filters are included for the ACS-WFC: F435W, F475W, F555W, F606W, F625W, F775W, F814W, and F850LP. The following filters are included for the WFPC2: F336W, F439W, F555W, F606W, F791W, F814W, and F850LP. The performance of the synthetic color transformation in the ACS F606W-F814W CMD has been documented by Sarajedini et al. (2007); Dotter et al. (2007); Richer et al. (2007); Siegel et al. (2007).

4.3. The Sloan Digital Sky Survey

SDSS produced (and its ongoing extensions continue to produce) vast quantities of stellar photometry and spectroscopy with important implications for our knowledge of galactic structure and evolution. The SDSS ugriz photometric system is based on the AB magnitude system but each of the five filters has an additional offset from AB of at most a few hundredths of a magnitude. The offsets, in the sense of mag(SDSS)–mag(AB) are: 0.04 in u, 0.01 in g, 0 in r, –0.015 in i, and –0.03 in z. The filter transmission curves and procedure for transforming synthetic fluxes to SDSS magnitudes magnitudes is outlined on the SDSS Photometric Flux Calibration web page [8].

Typically, the synthetic colors provide good fits to SDSS data in g, r, and i. Synthetic photometry in the u band is subject to the same shortcomings as other bands at bluer wavelengths while problems with the underlying calibration of the SDSS photometric systems persist in both u and z.

4.4. Semi–Empirical Transformations

For general use, and comparison with the synthetic color transformations, the tracks and isochrones are presented in colors based on the semi–empirical transformations of Vandenberg & Clem (2003, hereafter VC03) in BV(RI)$_C$. VC03 compiled a set of T$_{eff}$–color transformations and bolometric corrections covering a wide range of metallicity, T$_{eff}$, and log g. The VC03 colors are based on MARCS model atmospheres (Bell & Gustafsson 1978, 1989; Vandenberg & Bell 1985) for lower temperatures and Kurucz models (consistent with Castelli (1999)) for higher temperatures. The color transformations are semi–empirical in the sense that VC03 began with a collection of synthetic colors and then applied corrections to the colors, primarily for cooler MS stars approaching and above [Fe/H]=0, based on observational constraints from

---

[8]http://www.sdss.org/dr6/algorithms/fluxcal.html

open clusters, globular clusters, and field stars.

Clem et al. (2004) presented color transformations for the Strömgren uvby photometric system. Clem et al. (2004) used a similar approach to VC03 by adopting MARCS models (Houdashelt et al. 2000) for $T_{eff} < 8,000$ K and colors based on Kurucz models (Castelli et al. 1997) for higher temperatures. The uvby color transformations of Clem et al. (2004) provide much better fits to observations than any synthetic color tables (see that paper for a detailed discussion) and thus no synthetic Strömgren photometry has been provided.

5.   Comparisons

This section will compare the DSEP models to comparable models and observational data from the literature. Dotter et al. (2007) presented comparisons with old, metal–poor isochrones (12 Gyr, Z=0.0001) from several groups and compared the DSEP isochrones to ACS photometry of two globular clusters: M 92 and 47 Tuc from the ACS Galactic Globular Cluster Survey (Sarajedini et al. 2007). As a result, this section will focus on model comparisons at [Fe/H] $\geq$ 0, along with younger, more metal rich open clusters. The one exception is a comparison of SDSS photometry from M 13 and NGC 2420 to the ugriz isochrones in §5.2.6.

5.1.   Comparisons with Other Models

Following Dotter et al. (2007), comparison isochrones were drawn from Pietrinferni et al. (2004, 2006); Cordier et al. (2007, hereafter BaSTI), Girardi et al. (2000, hereafter Padova), Vandenberg et al. (2006, hereafter Victoria-Regina (VR)), and Yi et al. (2003, 2004, hereafter Yale-Yonsei (Y^2)). In this section, the comparison is extended to solar metallicity and above as well as to younger ages. Comparisons are shown in both the log T_{eff}-log $L/L_\odot$ plane and the V vs. V–I color-magnitude diagram. In each case, the DSEP isochrone is shown with the synthetic color transformation. A comparison of different color transformations applied to the DSEP isochrones appears later in this section.

Figures 2 and 3 show isochrones at [Fe/H] $\sim$+0.15 and an age of 625-630 Myr (compatible with the the Hyades, see §5.2.2). The isochrones range in initial Z=0.025 to 0.03 and Y=0.28 to 0.3. In Figure 2, the Padova, BaSTI, and DSEP isochrones all show the AGB though the point at which the AGB terminates differs: DSEP and BaSTI stop at or before the onset of thermal pulsations though the BaSTI library has been updated to include extended AGB evolution (Cordier et al. 2007). Fainter than log $L/L_\odot$=−1, the large
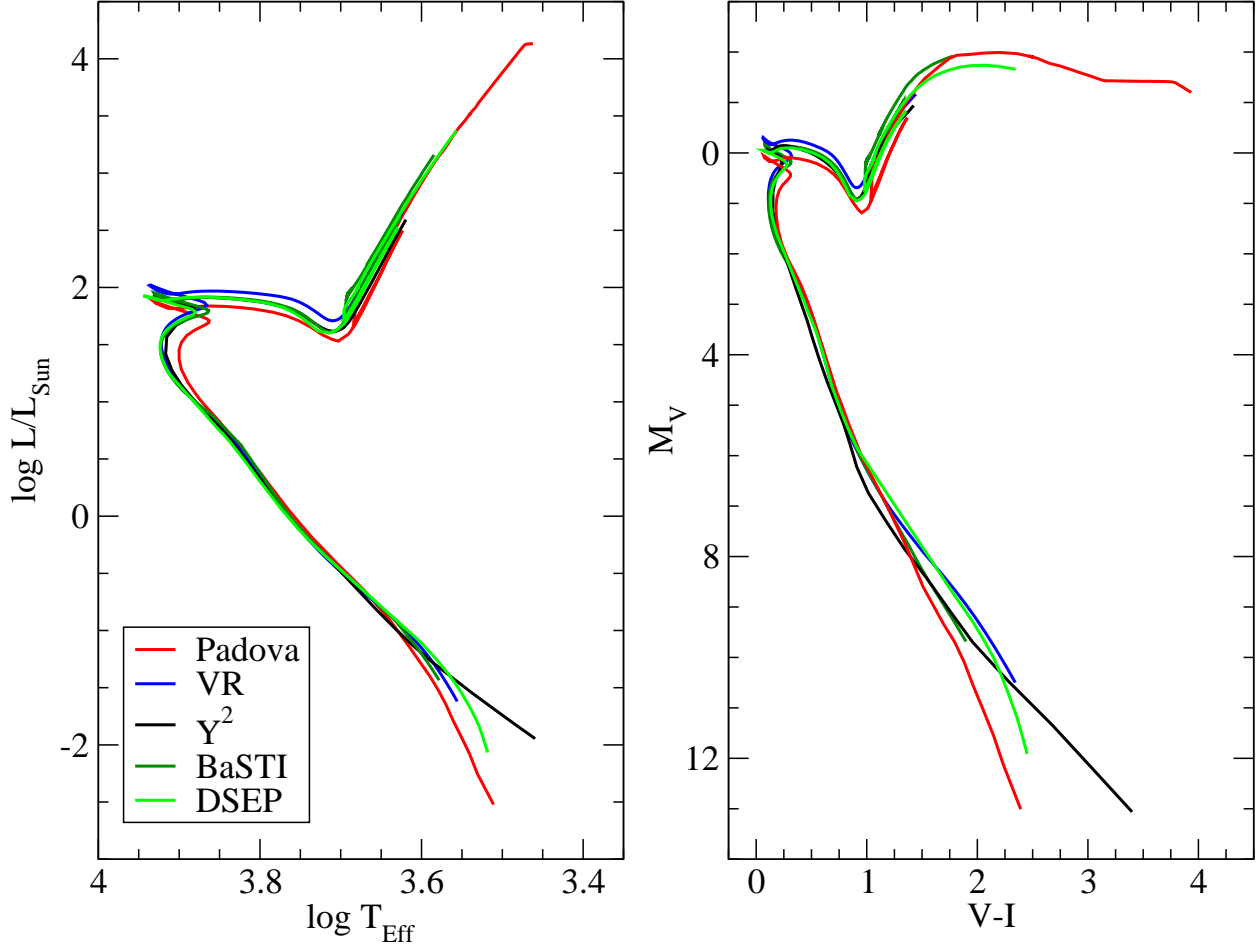
Fig. 2.— A plot of isochrones at [Fe/H] ∼+0.15 and an age of ∼ 625 Myr. The Padova, BaSTI, and DSEP isochrones show the He burning phase but the others do not. Good agreement exists among all the isochrones except for Padova that is cooler and fainter around the main sequence turn off.

Table 1.   Minimum Mass (M$_\odot$) for Convective Core Overshoot

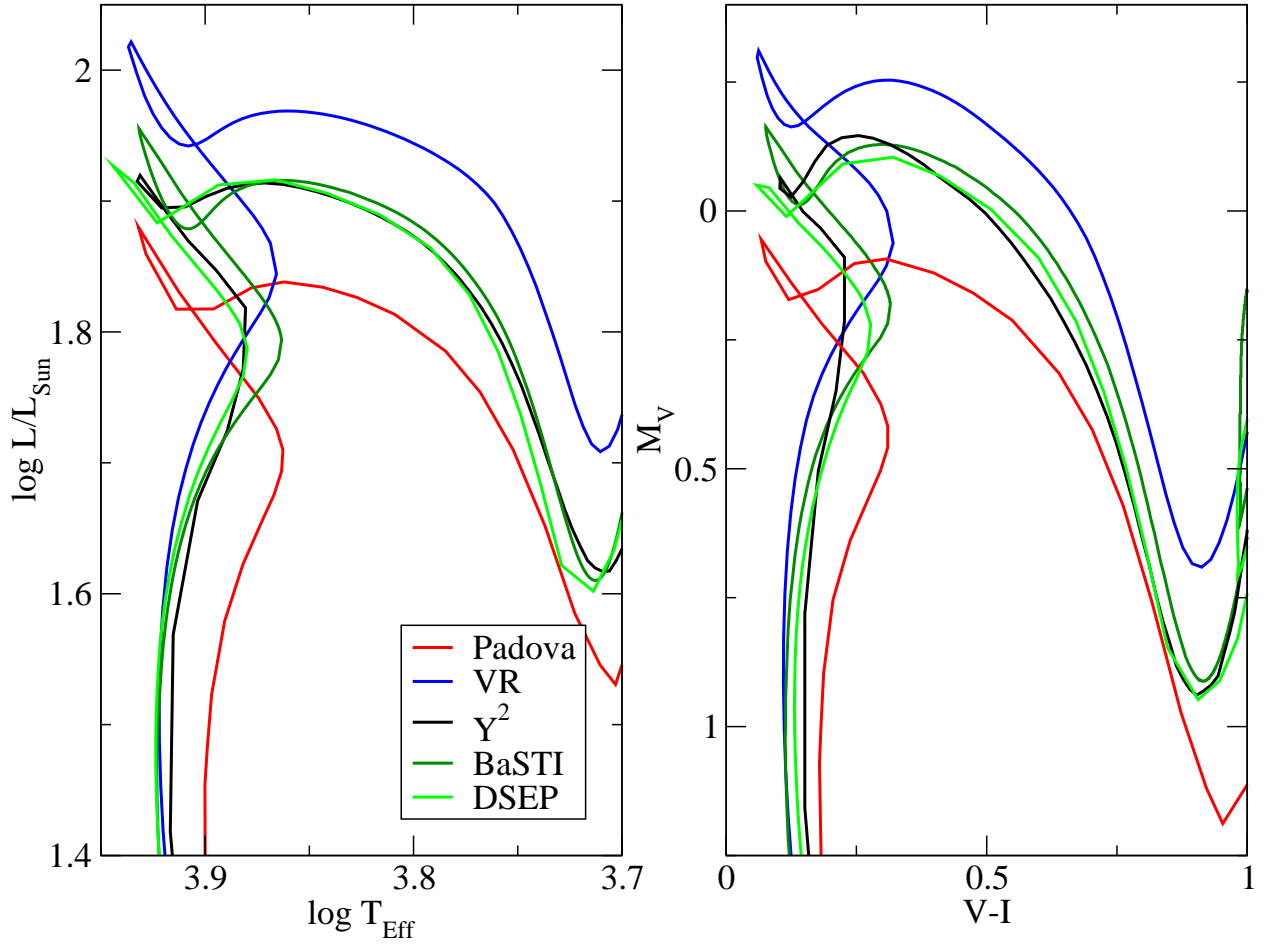| [Fe/H]	[α/Fe]=−0.2	Y=0.245+1.54Z					Y=0.33		Y=0.4	
		0	0.2	0.4	0.6	0.8	0	0.4	0	0.4
−2.5	1.6	1.6	1.6	1.5	1.3	1.3	1.5	1.5	1.5	1.5
−2.0	1.4	1.4	1.4	1.4	1.3	1.3	1.5	1.5	1.5	1.5
−1.5	1.4	1.4	1.4	1.4	1.3	1.3	1.4	1.4	1.4	1.4
−1.0	1.4	1.4	1.4	1.4	1.2	1.2	1.4	1.4	1.4	1.4
−0.5	1.2	1.2	1.2	1.2	1.2	1.0	1.2	1.2	1.2	1.2
0.0	1.2	1.2	1.1	1.1	1.0	0.9	1.2	1.1	1.2	1.1
+0.15	$\cdots$	1.1	$\cdots$	$\cdots$	$\cdots$	$\cdots$	$\cdots$	$\cdots$	$\cdots$	$\cdots$
+0.3	1.1	1.1	1.1	$\cdots$	$\cdots$	$\cdots$	$\cdots$	$\cdots$	$\cdots$	$\cdots$
+0.5	1.1	1.1	1.0	$\cdots$	$\cdots$	$\cdots$	$\cdots$	$\cdots$	$\cdots$	$\cdots$

Fig. 3.— The same as Figure 2 but focused on the region near the main sequence turn off.

Table 2.   Mass Fractions of Z

| Element | [α/Fe]= | | | | | |
	−0.2	0	0.2	0.4	0.6	0.8
C	2.296E-01	1.721E-01	1.233E-01	8.490E-02	5.685E-02	3.731E-02
N	6.726E-02	5.041E-02	3.611E-02	2.487E-02	1.665E-02	1.093E-02
O	3.940E-01	4.680E-01	5.314E-01	5.800E-01	6.155E-01	6.403E-01
Ne	9.044E-02	1.050E-01	1.165E-01	1.271E-01	1.349E-01	1.403E-01
Na	2.773E-03	2.078E-03	1.489E-03	1.025E-03	6.866E-04	4.506E-04
Mg	3.366E-02	3.998E-02	4.540E-02	4.955E-02	5.258E-02	5.470E-02
Al	4.814E-03	3.608E-03	2.585E-03	1.780E-03	1.192E-03	7.822E-04
Si	3.715E-02	4.412E-02	5.010E-02	5.468E-02	5.803E-02	6.036E-02
P	6.493E-04	4.866E-04	3.486E-04	2.401E-04	1.607E-04	1.055E-04
S	1.851E-02	2.199E-02	2.497E-02	2.725E-02	2.892E-02	3.008E-02
Cl	3.900E-04	2.923E-04	2.094E-04	1.442E-04	9.656E-05	6.337E-05
Ar	5.793E-03	4.342E-03	3.111E-03	2.142E-03	1.434E-03	9.414E-04
K	3.045E-04	2.282E-04	1.635E-04	1.126E-04	7.539E-05	4.948E-05
Ca	3.268E-03	3.882E-03	4.408E-03	4.811E-03	5.106E-03	5.311E-03
Ti	1.519E-04	1.804E-04	2.048E-04	2.236E-04	2.372E-04	2.468E-04
Cr	1.470E-03	1.102E-03	7.894E-04	5.436E-04	3.640E-04	2.389E-04
Mn	1.075E-03	8.054E-04	5.771E-04	3.974E-04	2.661E-04	1.746E-04
Fe	1.020E-01	7.641E-02	5.474E-02	3.770E-02	2.524E-02	1.657E-02
Ni	6.026E-03	4.516E-03	3.235E-03	2.228E-03	1.492E-03	9.791E-04

Table 3.   Initial Compositions

[Fe/H]	[α/Fe]=−0.2	Y=0.245+1.54Z					Y=0.33		Y=0.4	
		0	0.2	0.4	0.6	0.8	0	0.4	0	0.4
−2.5	X=0.7549	0.7548	0.7548	0.7547	0.7546	0.7543	0.6699	0.6699	0.6000	0.5999
	Z=4.09E-5	5.48E-5	7.63E-5	1.11E-4	1.65E-4	2.52E-4	4.85E-5	9.85E-5	4.34E-5	8.82E-5
−2.0	X=0.7547	0.7545	0.7544	0.7541	0.7536	0.7529	0.6698	0.6697	0.5999	0.5997
	Z=1.30E-4	1.72E-4	2.41E-4	3.50E-4	5.24E-4	7.97E-4	1.53E-4	3.50E-4	1.37E-4	2.79E-4
−1.5	X=0.7539	0.7536	0.7530	0.7521	0.7507	0.7484	0.6695	0.6690	0.5996	0.5991
	Z=4.10E-4	5.47E-4	7.62E-4	1.11E-3	1.65E-3	2.50E-3	4.85E-4	9.83E-4	4.34E-4	8.81E-4
−1.0	X=0.7516	0.7505	0.7487	0.7459	0.7415	0.7346	0.6685	0.6669	0.5986	0.5972
	Z=1.29E-3	1.72E-3	2.40E-3	3.46E-3	5.15E-3	7.77E-3	1.53E-3	3.46E-3	1.37E-3	2.78E-3
−0.5	X=0.7444	0.7441	0.7355	0.7270	0.7139	0.6942	0.6652	0.6603	0.5957	0.5913
	Z=4.05E-3	5.37E-3	7.44E-3	1.07E-2	1.57E-2	2.32E-2	4.82E-3	9.70E-3	4.31E-3	8.69E-3
0.0	X=0.7174	0.7071	0.6882	0.6628	0.6247	0.5710	0.6550	0.6402	0.5866	0.5734
	Z=1.43E-2	1.89E-2	2.55E-2	3.52E-2	4.97E-2	7.02E-2	1.50E-2	2.98E-2	1.34E-2	2.66E-2
+0.15	X= ⋯	0.6880	⋯	⋯	⋯	⋯	⋯	⋯	⋯	⋯
	Z= ⋯	2.56E-2	⋯	⋯	⋯	⋯	⋯	⋯	⋯	⋯
+0.3	X=0.6842	0.6638	0.6334	⋯	⋯	⋯	⋯	⋯	⋯	⋯
	Z=2.70E-2	3.48E-2	4.64E-2	⋯	⋯	⋯	⋯	⋯	⋯	⋯
+0.5	X=0.6491	0.6185	0.5792	⋯	⋯	⋯	⋯	⋯	⋯	⋯
	Z=4.04E-2	5.21E-2	6.71E-2	⋯	⋯	⋯	⋯	⋯	⋯	⋯

Table 4.   Surface Compositions for ZAHB Models

[Fe/H]	[α/Fe]=−0.2	$Y_{init}=0.245+1.54Z_{init}$[†]					$Y_{init}=0.33$		$Y_{init}=0.4$	
		0	0.2	0.4	0.6	0.8	0	0.4	0	0.4
−2.5	X=0.7564	0.7565	0.7561	0.7549	0.7549	0.7546	0.6835	0.6828	0.5967	0.6212
	Z=3.97E-5	5.31E-5	7.40E-4	1.60E-4	1.08E-4	2.44E-4	4.63E-5	9.40E-5	8.40E-3	8.33E-5
−2.0	X=0.7547	0.7548	0.7551	0.7541	0.7524	0.7510	0.6820	0.6810	0.6208	0.6193
	Z=1.26E-4	1.67E-4	2.33E-4	3.41E-4	5.06E-4	7.69E-4	1.46E-4	2.97E-4	1.30E-4	2.64E-4
−1.5	X=0.7529	0.7517	0.7509	0.7491	0.7464	0.7427	0.6785	0.6763	0.6180	0.6156
	Z=3.96E-4	5.29E-4	7.37E-4	1.07E-3	1.60E-3	2.43E-3	4.64E-4	9.44E-4	4.12E-4	8.37E-4
−1.0	X=0.7472	0.7453	0.7423	0.7383	0.7325	0.7238	0.6732	0.6698	0.6125	0.6076
	Z=1.25E-3	1.67E-3	2.33E-3	3.37E-3	5.02E-3	7.59E-3	1.47E-3	3.00E-3	1.31E-3	2.67E-3
−0.5	X=0.7350	0.7309	0.7242	0.71485	0.7010	0.6810	0.6641	0.6600	0.6034	0.5967
	Z=3.94E-3	5.24E-3	7.27E-3	1.05E-2	1.54E-3	2.28E-2	4.67E-3	9.48E-3	4.16E-3	8.41E-3
0.0	X=0.7166	0.6928	0.6741	0.6497	0.6131	0.5640	0.6477	0.6303	0.5877	0.5854
	Z=1.41E-2	1.85E-2	2.50E-2	3.46E-2	4.88E-2	6.87E-2	1.47E-2	2.91E-2	1.31E-2	2.68E-2
+0.15	X= ···	0.6737	···	···	···	···	···	···	···	···
	Z= ···	2.51E-2	···	···	···	···	···	···	···	···
+0.3	X=0.6696	0.6505	0.6204	···	···	···	···	···	···	···
	Z=2.66E-2	3.42E-2	4.57E-2	···	···	···	···	···	···	···
+0.5	X=0.6360	0.6075	0.5734	···	···	···	···	···	···	···
	Z=3.98E-2	5.12E-2	6.57E-2	···	···	···	···	···	···	···

[†]Y_{init} and Z_{init} refer to the initial Y and Z values, for the initial compositions see Table 3.

differences are due to different mass ranges, the EOS, and low temperature opacities used by each group. The BaSTI isochrone begins at 0.5 $M_\odot$, VR and Y^2 isochrones begin at 0.4 $M_\odot$, the Padova isochrone begins at 0.15 $M_\odot$, and the DSEP isochrone begins at 0.3 $M_\odot$ at this age.

In Figure 3 the agreement is quite good among DSEP, BaSTI, and Y^2 isochrones. The Padova isochrone is less luminous in the region of the MS and subgiant branch (SGB) while the VR isochrons is more luminous in the same region. These differences in luminosity are primarily due to different adopted treatment of convective core overshoot.

Figure 2 indicates that the Y^2 isochrone extends to cooler temperatures than any of the others despite the fact that it terminates at 0.4 $M_\odot$ while DSEP and Padova terminate at considerably lower mass. This effect is almost certainly due to the EOS used in the Y^2 calculations.

Figures 4 and 5 show isochrones at solar metallicity and 4 Gyr (compatible with M 67, see §5.2.4). Each isochrone has an initial Z=0.018-0.020 and Y=0.27-0.28; the adopted physics (especially the EOS and convective core overshoot prescription) and solar heavy element mixture differ from one group to another. In the left panels of Figure 4 and 5, the isochrones are in reasonable agreement for points brighter than log $L/L_\odot$=–1 (Padova and BaSTI isochrones include He burning stars while the others do not). In Figure 5, the BaSTI, VR, and DSEP isochrones all agree well on the temperature and luminosity of the MS turn off (TO) and SGB. In the right panels of Figure 4 and 5, all isochrones agree well at magnitudes brighter than M_V=6 except for Padova that is consistently redder and brighter on the upper RGB. In Figure 4 the DSEP isochrone includes the complete lower mass range (down to 0.1 $M_\odot$) and the fact that the Y^2 isochrone is cooler and almost as faint in M_V is significant. Conversely, the Padova isochrone is hotter and bluer than the others for points fainter that log $L/L_\odot$=–1 (M_V=7) although the mass-luminosity relation is similar to the DSEP isochrone.

Figures 2, 3, 4 and 5 show general agreement amongst the different sets of isochrones. The main exceptions are the Padova isochrones that appear cooler and redder near the MSTO and on the RGB but hotter and bluer on the lower main sequence. Amongst the other models the largest differences occur near the MSTO where the adopted core overshoot treatments differ and on the lower main sequence where the adopted EOS and minimum masses differ. The DSEP models use the same EOS and opacities as the VR and BaSTI models and it is reassuring that these models all lie close together aside from the noted exceptions due to the included mass range and treatment of convective core overshoot.
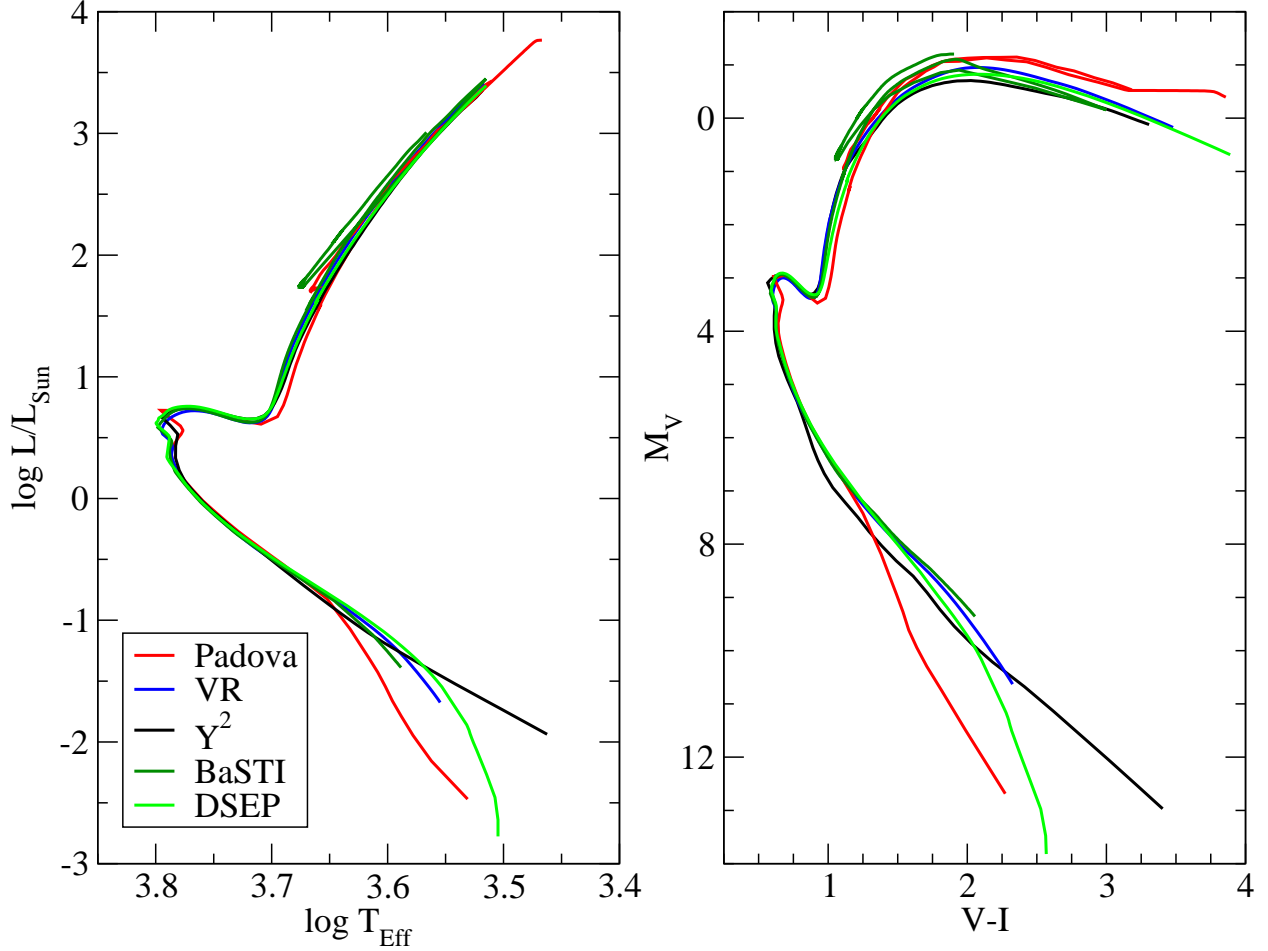
Fig. 4.— The figure shows solar metallicity isochrones at 4 Gyr. The Padova and BaSTI isochrones include the He burning phase but the others do not. There is remarkable agreement in the H–R diagram between the tip of the red giant branch and log L/L$_\odot$=−1. Below this point, the range of masses plotted and the adopted EOS cause large differences. There is good agreement in the color-magnitude diagram between M$_V$=6 and 0 but beyond this the mass range plotted, the underlying physics, and the choice of color transformation cause significant discrepancies.

Table 5.   He Core Mass (M$_\odot$) for ZAHB Models

[Fe/H]	[α/Fe]=−0.2	Y=0.245+1.54Z					Y=0.33		Y=0.4	
		0	0.2	0.4	0.6	0.8	0	0.4	0	0.4
−2.5	0.506	0.505	0.504	0.502	0.500	0.497	0.489	0.485	0.474	0.473
−2.0	0.500	0.499	0.498	0.494	0.492	0.491	0.483	0.479	0.469	0.468
−1.5	0.495	0.493	0.491	0.489	0.488	0.486	0.478	0.474	0.464	0.463
−1.0	0.489	0.488	0.486	0.484	0.481	0.478	0.473	0.469	0.460	0.458
−0.5	0.483	0.482	0.480	0.477	0.473	0.469	0.469	0.465	0.457	0.455
0.0	0.475	0.473	0.469	0.464	0.458	0.447	0.465	0.460	0.454	0.451
+0.15	$\cdots$	0.468	$\cdots$	$\cdots$	$\cdots$	$\cdots$	$\cdots$	$\cdots$	$\cdots$	$\cdots$
+0.3	0.468	0.464	0.459	$\cdots$	$\cdots$	$\cdots$	$\cdots$	$\cdots$	$\cdots$	$\cdots$
+0.5	0.461	0.456	0.449	$\cdots$	$\cdots$	$\cdots$	$\cdots$	$\cdots$	$\cdots$	$\cdots$
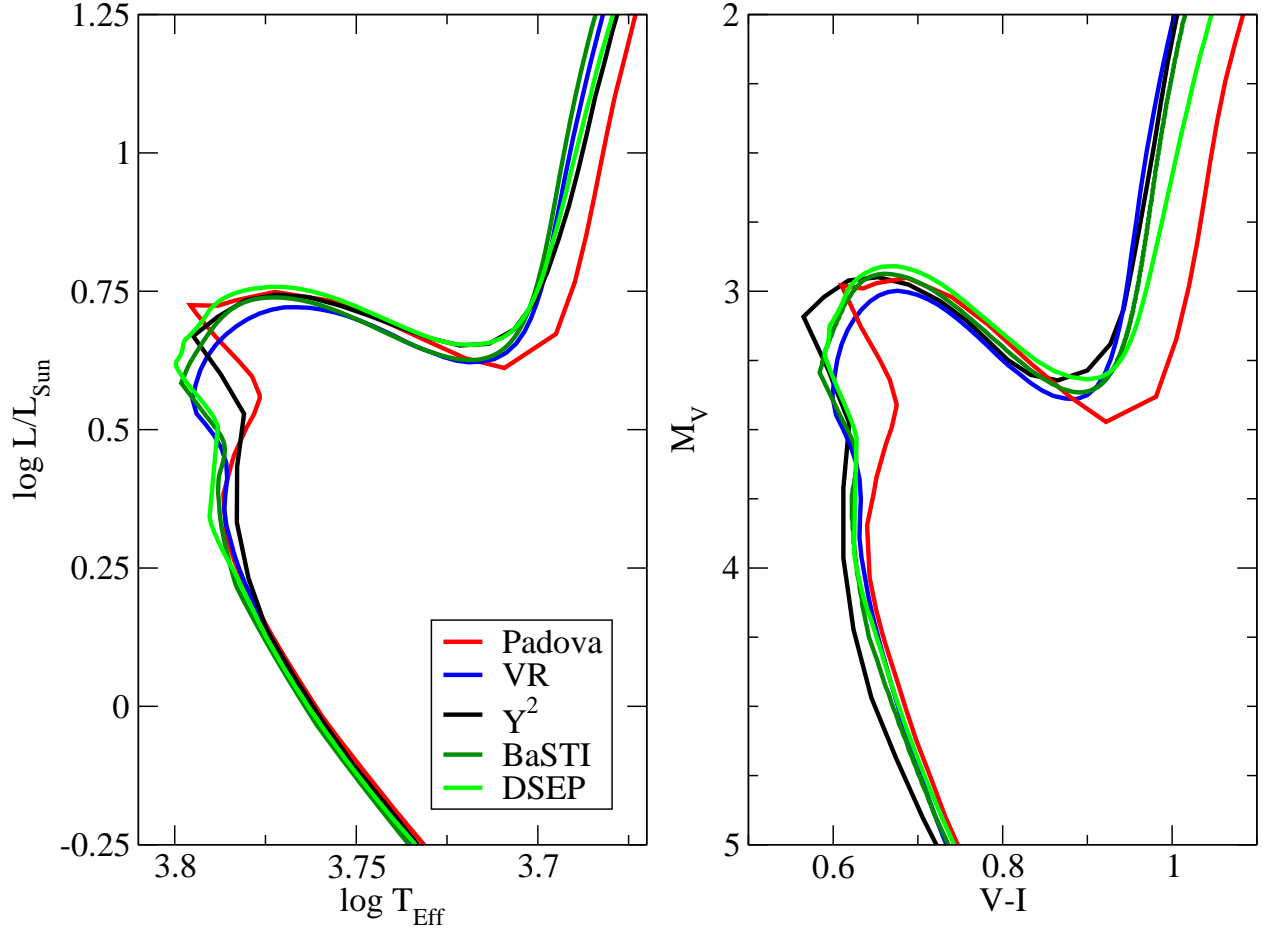
Fig. 5.— The same as Figure 4 but focused on the region near the main sequence turn off.

5.2. Comparisons with Observational Data

Several papers have demonstrated the performance of the DSEP isochrones when applied to HST/ACS data in two of the most popular bands for globular cluster photometry (F606W and F814W) including: Sarajedini et al. (2007), Dotter et al. (2007), Siegel et al. (2007), and Richer et al. (2007). This section will focus on the ground-based photometric systems presented in this paper and also compares the synthetic color transformation with the VC03 transformation in B–V and V–I.

Grocholski & Sarajedini (2003, hereafter GS03) combined optical photometry of six Galactic open clusters with near-infrared data from 2MASS. Similar compilations for the Hyades (Pinsonneault et al. 2004) and NGC 6791 (Carney et al. 2005) are presented along with three clusters from GS03 to span a range of ages and metallicities in open clusters. These combined optical and near-infrared data provide an excellent source of comparisons with the DSEP isochrones. Table 6 lists the relevant parameters of the clusters featured in this section.

The adopted reddening values are listed as E(B–V). The extinction curve of Johnson (1965) was used to determine the reddening in other filter combinations: E(V–I) = 1.4 E(B–V), E(V–J) = 2.4 E(B–V) and E(V-K_s) = 2.8 E(B–V).

These comparisons are not meant to determine the ages of the clusters but rather to demonstrate the performance of the isochrones. The ages were chosen to be consistent with other published results but if the age shown is considerably different from the true age of the cluster it will influence the quality of the fit.

5.2.1. M 37

Figure 6 shows the CMD of M 37 in B–V (Kalirai et al. 2001) and V–J and V–K_s (GS03) along with a [Fe/H]=0, 500 Myr isochrone. The isochrone is plotted using the synthetic (solid line) and VC03 (dashed line) colors.

In B–V (left panel of Figure 6), the synthetic color isochrone is redder than the data by ∼0.1 mag throughout the CMD while the VC03 isochrone provides a reasonable fit to the data from the MSTO to V=16 before drifting to the red of the data. The He burning portion of the isochrone is redder than the data by 0.1 mag in both color transformations.

In V–J and V–K_s, the synthetic color isochrone provides an excellent fit to the data for the entire extent of the MS (the MS data cuts off at V∼20 in V–J and V–K_s). The isochrone is redder than the data for the He burning stars in both V–J and V–K_s.
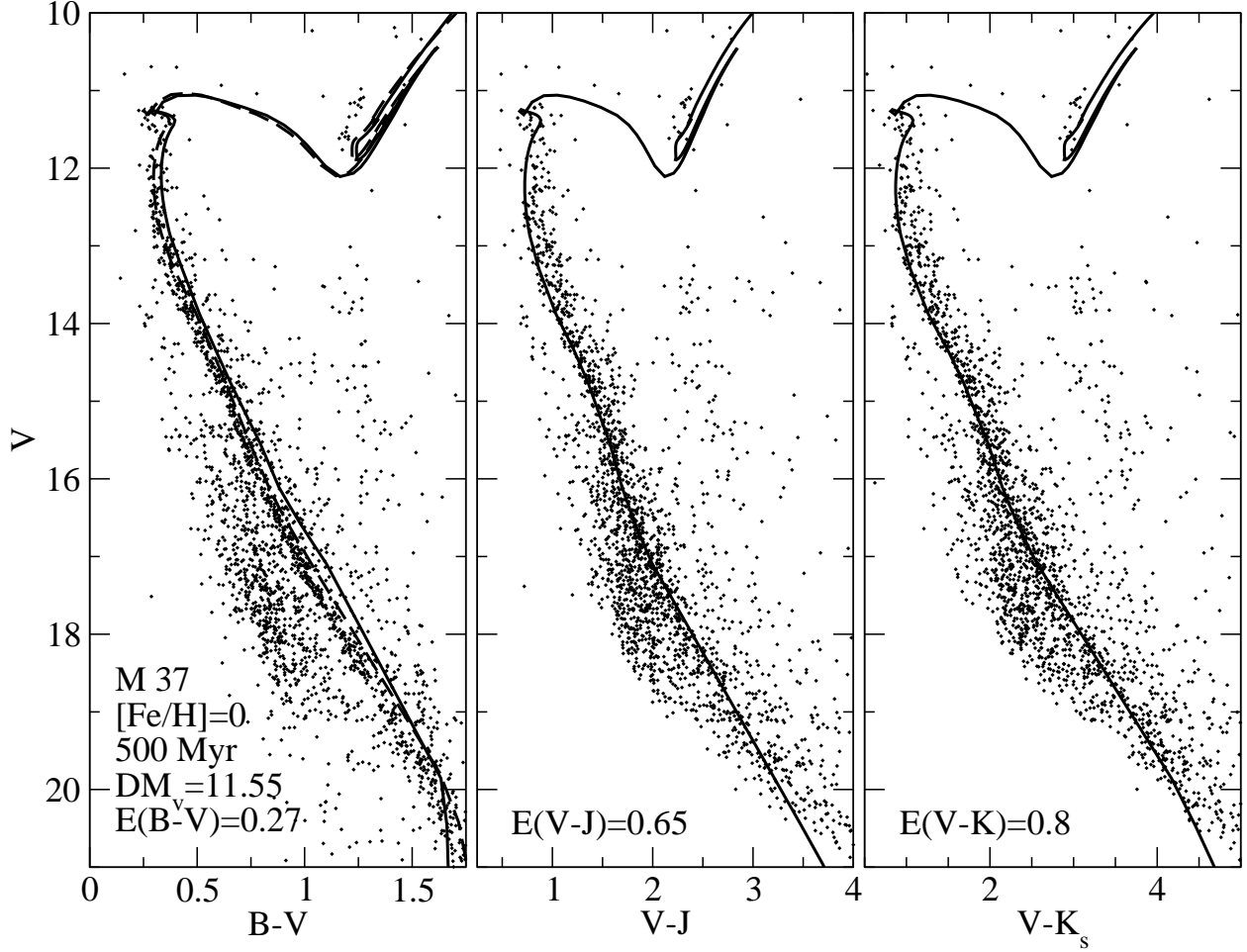
Fig. 6.— CMDs of M 37 from Kalirai et al. (2001) and GS03 are plotted with a [Fe/H]=0, 500 Myr isochrone. The isochrone is shown in synthetic (solid line) and VC03 (dashed line) colors. The synthetic color isochrone is redder than the data in B–V but a good fit in V–J and V–K$_s$. The He burning portion of the isochrones is redder than the data in all cases.

We note in passing that the VC03 B–V isochrone shown in the left panel of figure 6 does not match the shape of the CMD for V > 17. Although M 37 and M 67 are both roughly [Fe/H] = 0 clusters their B–V CMDs from Kalirai et al. (2001) and M 67 (Montgomery et al. 1994), respectively, adjusted for distance and reddening, appear to disagree somewhat for $M_V \gtrsim 6$ when viewed together. Since the VC03 colors are based in part on the CMD of M 67, it is impossible for them to fit both clusters simultaneously.

5.2.2. The Hyades

Figure 7 shows the Hipparcos B–V (left panel) and V–I (center) CMDs of the Hyades (de Bruijne et al. 2001) and the combined Hipparcos and 2MASS V–K_s CMD compiled by Pinsonneault et al. (2004). Along with the data, a [Fe/H]=+0.15, 625 Myr isochrone is shown in the synthetic (solid line) and VC03 (dashed line) color transformations. The choice of a 625 Myr isochrone may be an underestimate of the age which is typically quoted as between 650 and 700 Myr (e.g. VC03). The He abundance assumed for the [Fe/H]=+0.15 models may also be a cause for disagreement since the adopted $\Delta Y/\Delta Z$ yields Y_{init}=0.2864 whereas the Hyades Y value inferred from model comparisons is lower by $\sim$0.02 (see VC03 and references therein for a discussion).

In B–V, the synthetic color isochrone is redder than the data by 0.05–0.1 mag down to M_V=7 where the slope changes and the isochrone becomes bluer than the data by M_V=8. The VC03 color isochrone, on the other hand, is a good fit for the entirety of the MS. Both isochrones appear cooler than the two He burning stars in the B–V CMD.

In V–I, the color transformations are quite similar and both perform well down to M_V=6. At this point, the isochrones become redder than the data before matching the data again at M_V=8.

In V–K_s, the synthetic color isochrone fits the data for stars with $M_V \geq 3$ but becomes bluer than the data just below the MSTO. The discrepancy just below the MSTO would be avoided by plotting a slightly older isochrone.

5.2.3. NGC 2420

Figure 8 shows the B–V, V–I, and V–K_s CMDs of NGC 2420 from GS03. Plotted along with the data is an isochrone interpolated to [Fe/H]=–0.25 and 2.15 Gyr. Given the adopted distance and reddening in Table 6, the best fit age plotted in Figure 8 is older than the age quoted by GS03. This is not surprising since ultimately the GS03 age estimate for
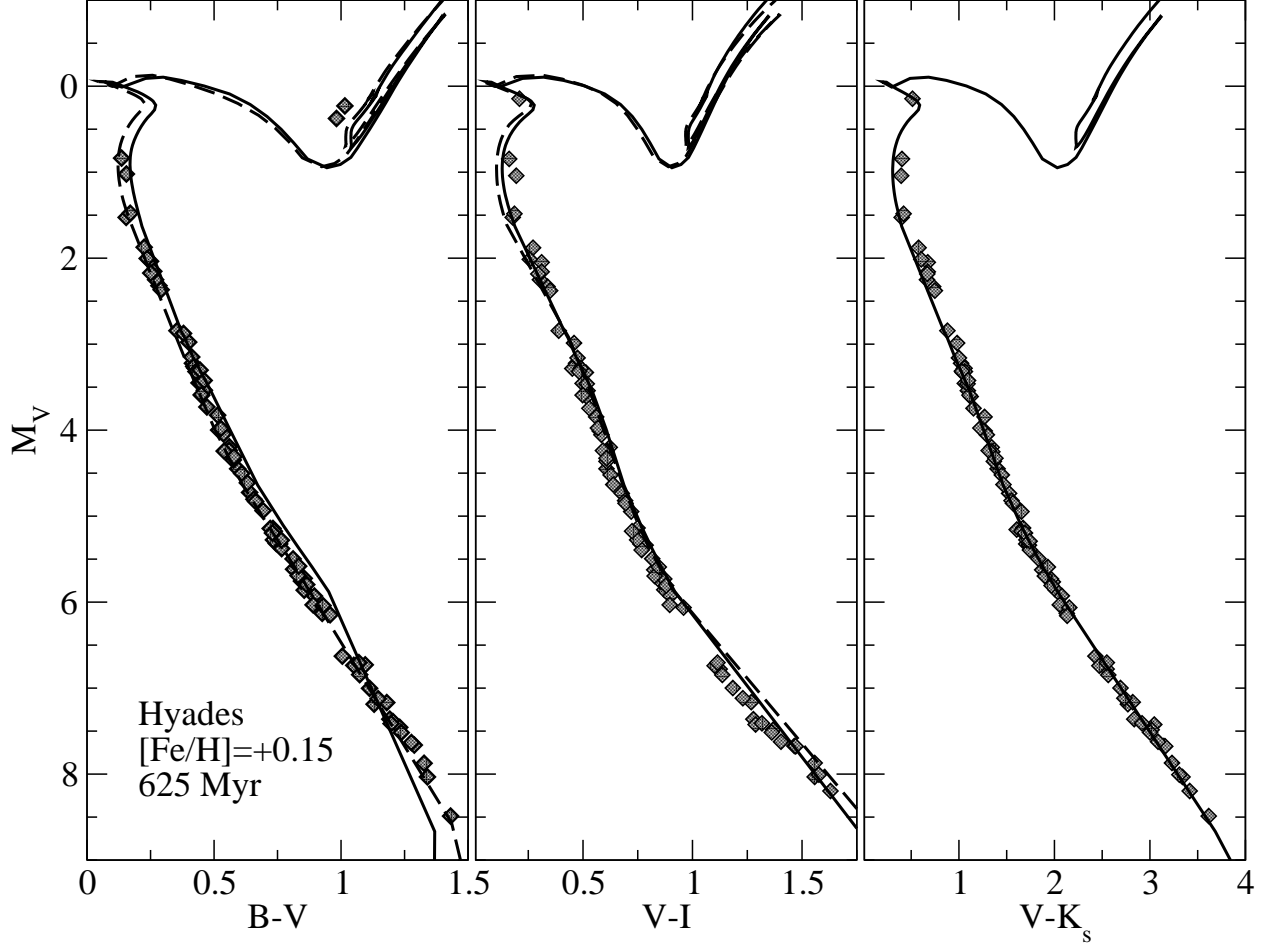
Fig. 7.— The Hyades in B–V and V–I from de Bruijne et al. (2001) along with V–K$_s$ from Pinsonneault et al. (2004). Along with the data, an isochrone with [Fe/H]=+0.15 at 625 Myr is plotted using the synthetic colors (solid line) and VC03 colors (dashed line).
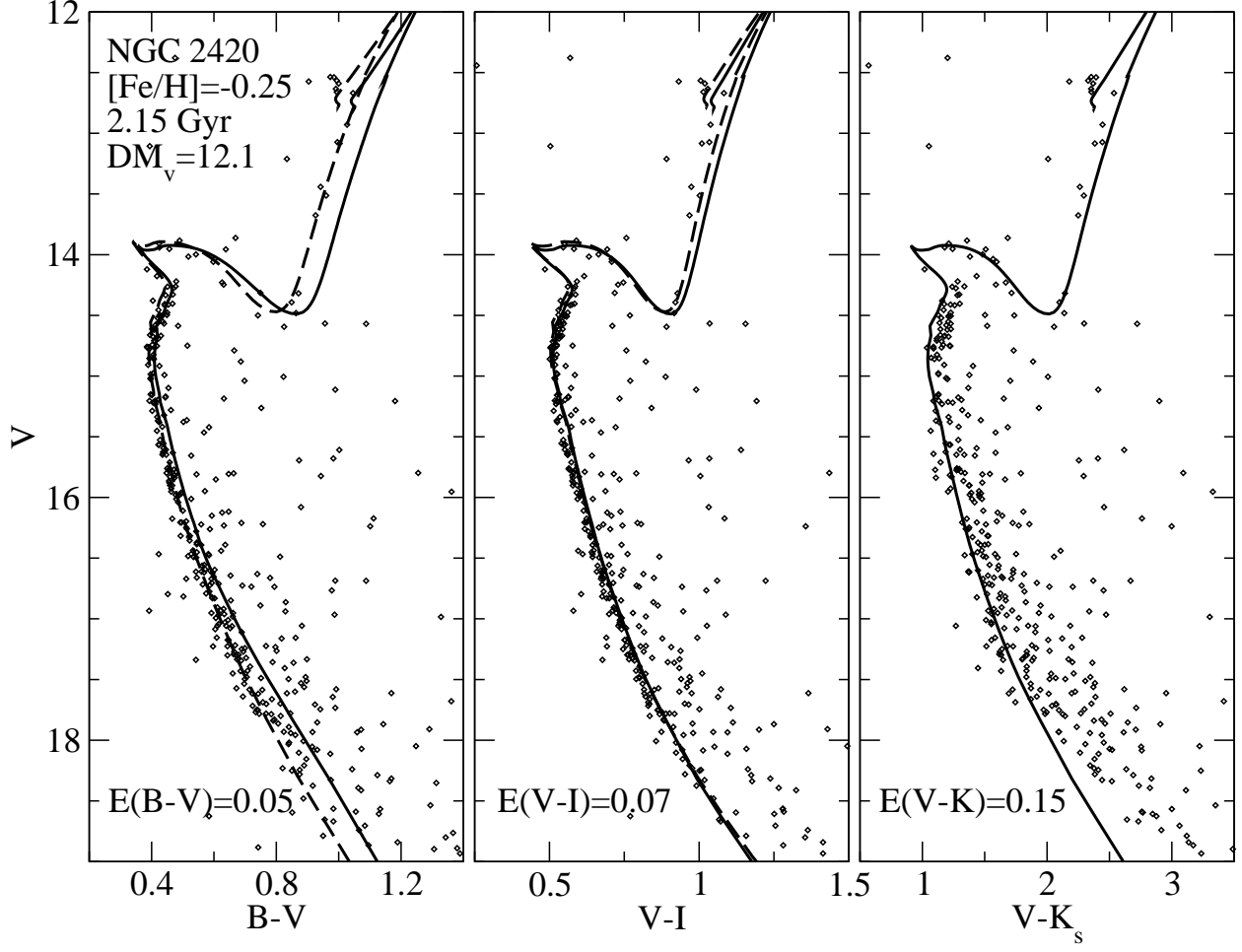
Fig. 8.— NGC 2420 from GS03 along with an isochrone interpolated to [Fe/H]=–0.25 and 2.15 Gyr. The isochrone is shown with synthetic colors (solid line) and VC03 colors (dashed line). Also shown is a 1.5 $M_\odot$ He burning track interpolated to [Fe/H]=–0.25.

NGC 2420 was based on Padova isochrones and these were shown to be fainter and redder near the MSTO than the DSEP isochrones (see Figures 2 and 4 and the discussion in §5.1). As a result, the best fit Padova isochrone will be younger than the best fit DSEP isochrone.

In B–V the synthetic isochrone is redder than the data, particularly on the lower MS and the RGB, though it matches well near the MSTO. The VC03 color isochrone fits the entire CMD well. The He burning track lies fainter than the red clump for both color transformations with the color predicted correctly by VC03 but too red by the synthetic color. If NGC 2420 is younger than 2.1 Gyr, then the stars in the red clump will be more massive and more luminous.

In V–I, both synthetic and VC03 colors fit the CMD well except for the synthetic color on the RGB that is slightly cooler than the data. The color of the red clump is correctly predicted by VC03 but slightly too red in the synthetic color.

In V–K$_s$, the synthetic isochrone fits the SGB and RGB and correctly predicts the color of the red clump. However, the V–K$_s$ color appears to be too blue on the MS.

5.2.4. M 67

Figure 9 shows the B–V, V–I, and V–K$_s$ CMDs of M 67 from Montgomery et al. (1994) and GS03 along with a [Fe/H]=0, 4 Gyr isochrone. The isochrone has been transformed using the synthetic (solid line) and VC03 (dashed line) colors. A He burning track with [Fe/H]=0 and M=1.25 M$_\odot$ is shown to indicate the predicted location of the red clump.

The fit of the synthetic color isochrone to the data in B–V (left panel of Figure 9) is poor, with the isochrone redder than the data by about 0.05-0.1 mag throughout the CMD while the VC03 color isochrone provides an excellent fit. The He burning model has the correct V magnitude but is slightly redder than the observed red clump in B–V for both color transformations.

In V–I (middle panel of Figure 9), both synthetic and VC03 colors match the data well over most of the CMD. The only exception is that, for stars fainter than V=17, the VC03 colors are redder than the data while the synthetic colors follow the data closely down to V=20. The He burning model correctly predicts the color of the red clump in V–I for both color transformations.

In V–K$_s$ only the synthetic color isochrone is plotted in the right panel of Figure 9. As with V–I, the synthetic V–K$_s$ color is an excellent fit to the data for the lower MS, the MSTO, the RGB, and the location of the red clump.
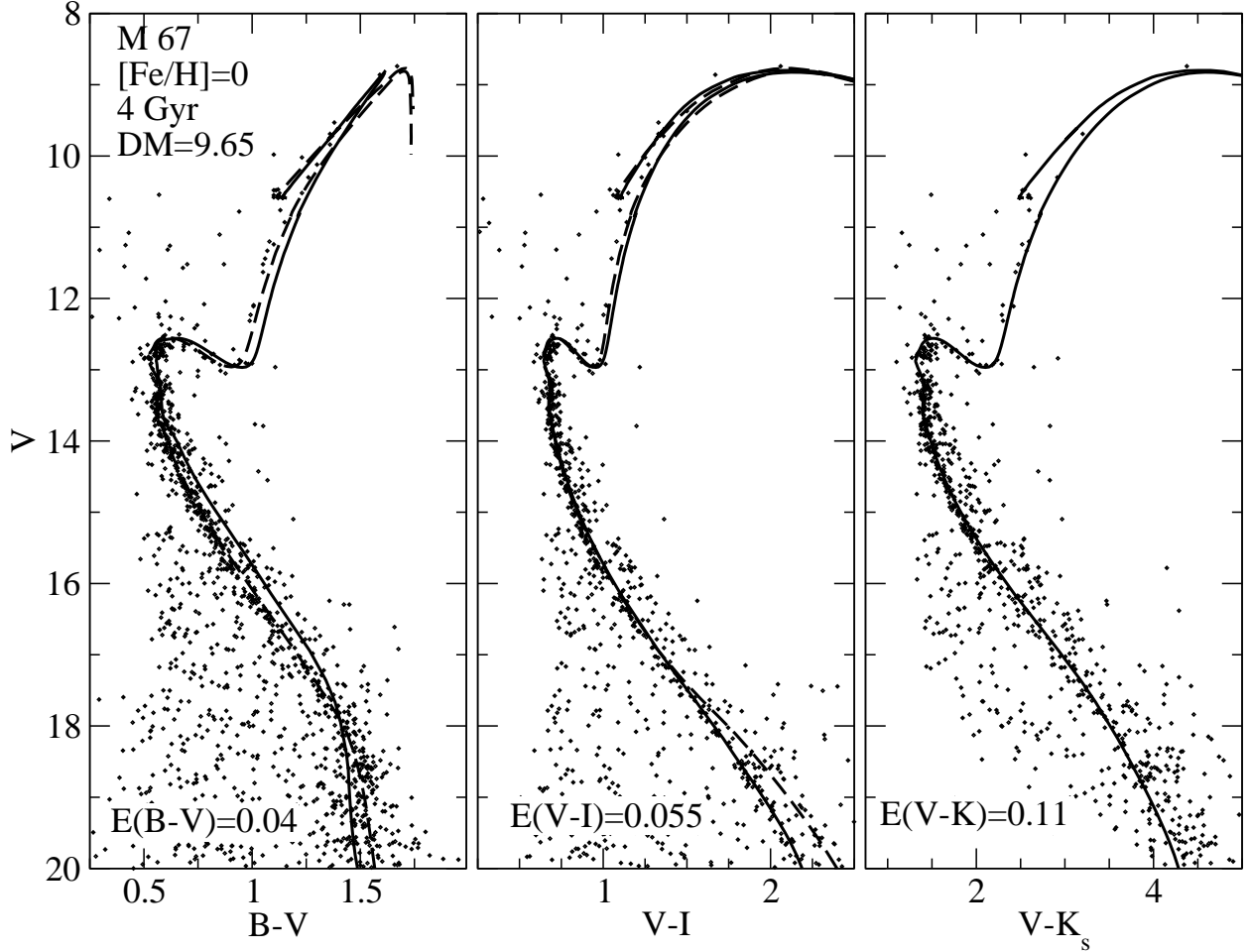
Fig. 9.— The CMDs of M 67 in B–V and V–I (Montgomery et al. 1994) and V–K$_s$ (GS03). Isochrones with [Fe/H]=0 at 4 Gyr are shown using synthetic (solid line) and VC03 (dashed line) colors. A He-burning track with M=1.25 M$_\odot$ at [Fe/H]=0 is plotted to indicate the predicted level of the red clump.

5.2.5. NGC 6791

Carney et al. (2005) combined JHK photometry of NGC 6791 with optical data from Stetson et al. (2003). The resulting CMDs in B–V, V–I, and V–K are shown in Figure 10. The V–K CMD has been adjusted by +0.024 mag to convert from CIT K to 2MASS K_s (Carpenter 2001). The isochrones shown in Figure 10 have $[Fe/H]_{init} = +0.36$ and an age of 9 Gyr.

The B–V CMD continues to be problematic for the synthetic colors where, using the adopted E(B–V), the synthetic isochrone is ∼0.1 mag redder than the data. The isochrone with VC03 colors is a substantially better fit to the data. This is not surprising since the VC03 colors were calibrated at high metallicity with the Stetson et al. (2003) data. The V–I CMD is equally well fit by both synthetic and VC03 colors. The synthetic color isochrone in V–K is an excellent fit to the shape of the CMD as well.

For the isochrone used in Figure 10, neglecting mass loss, the mass at the tip of the RGB is 1.12 $M_\odot$. A 1 $M_\odot$ He burning track is plotted to show the predicted level of the red clump in Figure 10. The He burning track provides a good fit to the V mag of the red clump but lies a few hundredths of a magnitude redder than the red clump in B–V for both color transformations. In V–I, the color of the red clump is in excellent agreement with the model. In V–K, the model is bluer than the red clump by a few hundredths of a magnitude.

It should be noted that while the adopted reddening value is E(B–V) = 0.1, Carney et al. (2005) found E(B–V) = 0.14 at [Fe/H]=+0.4 and the Schlegel et al. (1998) dust maps yield E(B–V) = 0.155 for NGC 6791. These values are both higher than the adopted value of E(B–V) and would alter the isochrone fits shown in Figure 10.

If instead E(B–V) = 0.15 is adopted as the reddening then the isochrone fits require either younger age or lower metallcity (or both). Using the same isochrones (with $[Fe/H]_{init}$=+0.36) but with the larger reddening, a reasonably good fit is achieved at 8 Gyr but with an increased distance modulus of $DM_V = 13.45$. Reducing [Fe/H] to +0.2 introduces a substantial mismatch between the observed CMD and the models along the MS with the isochrones becoming bluer than the data at 2 mag below the MSTO.

Given that the adopted [Fe/H] value provides a good fit to the entire CMD and agrees with recent spectroscopic estimates by, for example, Carraro et al. (2006) and Origlia et al. (2006), the isochrones show a clear preference for the lower reddening value of E(B–V)=0.1 used in Figure 10. Constraining the distance, reddening, composition, and age of NGC 6791 remains a thorny problem (see Chaboyer et al. (1999) for a detailed discussion). Because of it high metallicity, a conclusive age determination of NGC 6791 will most likely require that the models follow the detailed abundance patterns found by spectroscopy and not simply
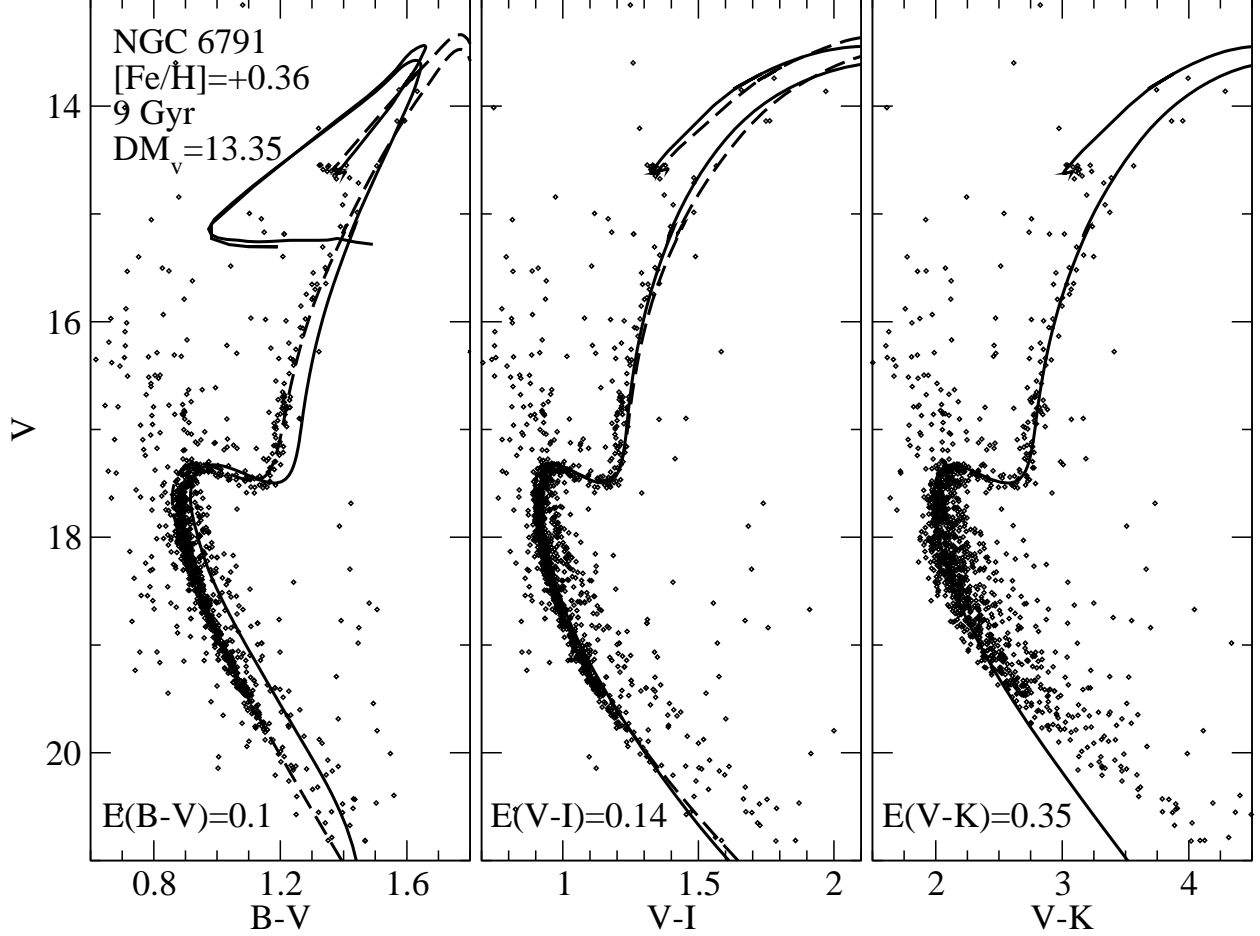
Fig. 10.— The B–V, V–I, V–K CMDs of NGC 6791 from Stetson et al. (2003) and Carney et al. (2005). Plotted on top of the data are isochrones with [Fe/H]=+0.36 at 9 Gyr in synthetic (solid line) and VC03 (dashed line) colors. A 1 M$_\odot$ He burning track of the same composition is plotted to indicate the predicted location of the red clump.

match the observed [Fe/H]. For example, Origlia et al. (2006) found that $[\alpha/\text{Fe}] \sim 0$ but [C/Fe]=–0.35 in NGC 6791.

5.2.6. Clusters in the SDSS ugriz system

Lee et al. (2007) present spectroscopically selected cluster members for stars in a sample of galactic globular and open clusters for purposes of validating the SEGUE Stellar Parameter Pipeline. The selected stars from M 13 and NGC 2420 are used here because they represent the cleanest available data sets of clusters on the SDSS ugriz system. Though these sequences are quite narrow and well–defined, they are not as deep as allowed by SDSS, but are suitable for the purpose of demonstrating the performance of the isochrones.

Figure 11 shows the g vs. $(g–i)_0$ CMDs of M 13 (left) and NGC 2420 (right) along with appropriate isochrones. The photometry has been de-reddened by Lee et al. (2007) using the Schlegel et al. (1998) dust maps. Plotted on top of the M 13 data in Figure 11 are isochrones with [Fe/H]=-1.5, $[\alpha/\text{Fe}]$=+0.2 at 11 and 13 Gyr assuming a distance modulus of 14.4 in agreement with Harris (1996). The isochrones follow the locus of stars on the MS and RGB well. The only real discrepancy is the slope of the SGB but this is a common problem with synthetic color isochrones compared to metal poor systems.

Plotted on top of the NGC 2420 data in Figure 11 is the same isochrone as in §5.2.3 but now transformed to g vs. g–i plane. The agreement between the data and the isochrone is excellent on the MS but the observational constraints of the sample do not permit comparison with stars in the convective hook or past the MSTO.

5.3. Discussion

Bluer synthetic colors, as represented by B–V in this section, continue to require adjustments in order to match observed CMDs as Figures 6 through 10 indicate. The semi-empirical color transformation of VC03 are an improvement over the synthetic B–V color but seem unnecessary for V–I when used in conjuction with the DSEP isochrones. While the synthetic colors and magnitudes are suitable analysis of observational data in bandpasses with central wavelengths longer than ~ 5000 Å, empirically adjusted colors ought to be used at shorter wavelengths. In these redder bands, the synthetic colors perform well throughout the CMD, including on the lower main sequence where they perform better than the empirical colors.

The optical to near-infrared comparisons in V–J (M 37 only) and V–K of the open clusters are favorable for entire extent of the MS and the RGB in the older clusters but
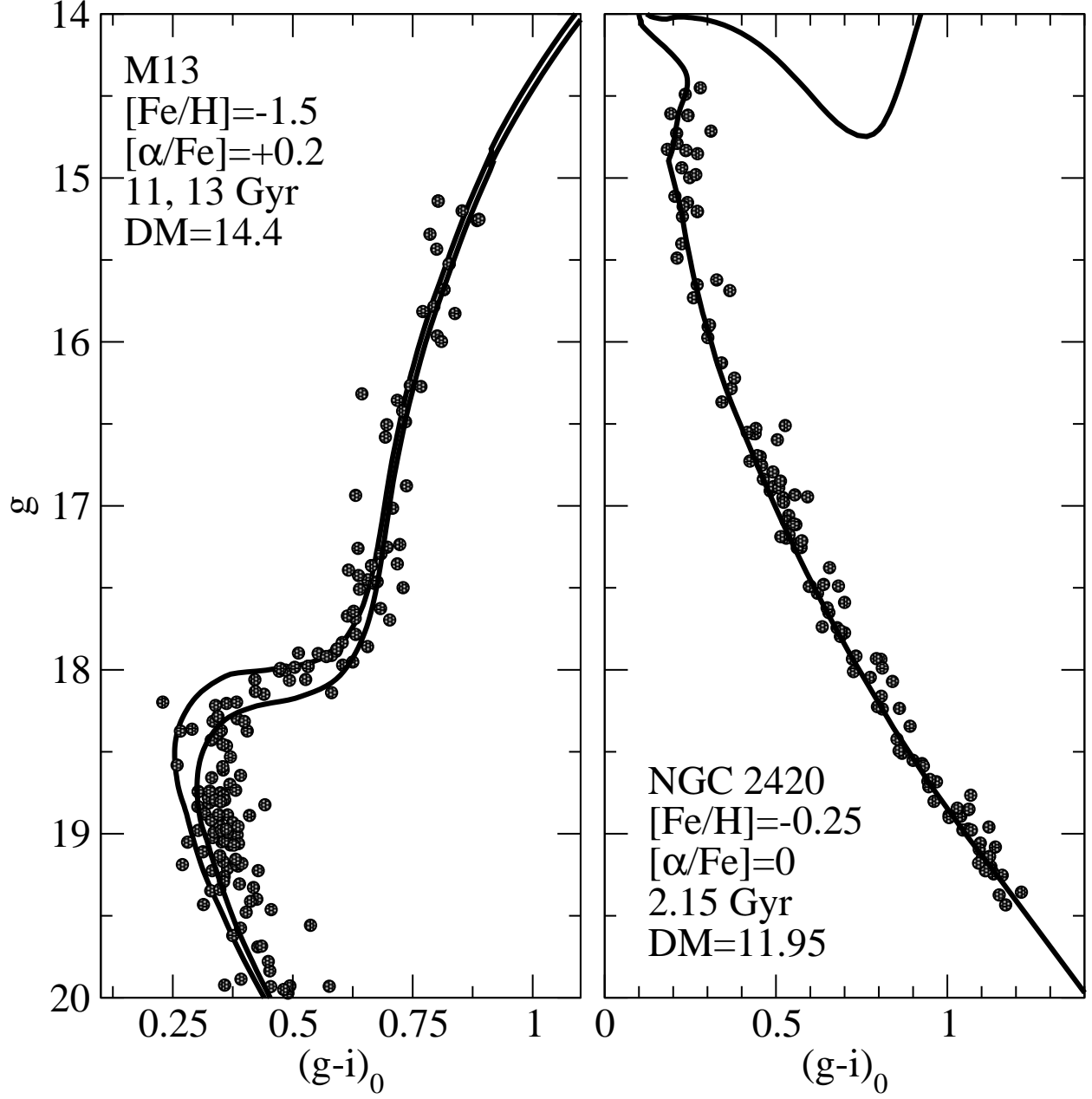
Fig. 11.— The de-reddened g–i CMDs of M 13 and NGC 2420 from Lee et al. (2007) plotted along with isochrones of appropriate age and metallicity transformed to the SDSS ugriz system.

larger reddening than suggested by the adopted reddening curve is needed in some cases.

The location of He burning stars in the open clusters is matched by the models in the older clusters (M 67 and NGC 6791) but for the younger clusters the models predict the red clump to be fainter (NGC 2420) and/or redder (M 37 and the Hyades) than the data suggest. The general lack of evolved stars in the CMDs of both M 37 and the Hyades makes it difficult to speculate as to whether the models are intrinsically too cool or whether the colors are too red for a given $T_{\rm eff}$.

6. Summary

The Dartmouth Stellar Evolution Program has been used to compute a large grid of stellar evolution tracks. A subset of these tracks and isochrones were presented by Dotter et al. (2007) and are extended in this paper to include younger ages, higher metallicities, and transformations to multiple photometric systems. These models take advantage of the latest advances in radiative opacities, nuclear reactions rate, and the equation of state.

The Dartmouth Stellar Evolution Database comprises a set of stellar evolution tracks and isochrones transformed to several photometric systems along with a set of computer programs that allow for interpolation and construction of luminosity functions and synthetic horizontal branch models. The database spans a wide range of compositions from [Fe/H]=–2.5 to +0.5, [α/Fe]=–0.2 to +0.8 (at [Fe/H] $\leq$0) or +0.2 (at [Fe/H] >0), and additional models with enhanced He for [Fe/H]=–2.5 to 0.

The models were transformed to the observational plane using a synthetic color transformation based on PHOENIX model atmospheres for $T_{\rm eff}$ <10,000 K and Castelli & Kurucz (2003) for hotter temperatures. The synthetic color transformations are compared to the VC03 semi-empirical transformations in B–V and V–I. The synthetic colors perform well in V–I but are consistently too red in B–V. As a general rule, the synthetic colors should only be trusted in bandpasses equivalent to V or redder, i.e. those with central wavelengths longer than ~ 5000 Å. In these bands, the synthetic colors were found to perform well—and better than the empirical colors— on the lower main sequence. Synthetic photometry in the bluer bandpasses (those with central wavelengths shorter than ~ 5000 Å) does not compare favorably with observations. Empirically adjusted magnitudes and colors should be favored for the bluer bandpasses whenever possible.

The isochrones were compared to isochrones from other groups at [Fe/H]=0 and +0.15 as well as photometry from open clusters and one globular cluster. The isochrones extend to lower mass (0.1 $M_{\odot}$) than those of other major isochrone libraries and provide reasonable

fits to the MS of the clusters shown in §5.

The Dartmouth Stellar Evolution Database should prove useful in studies of resolved stellar populations in the local Universe and is suitable for application to population synthesis and integrated light models. The database is available through a dedicated website.

REFERENCES

Adelberger, E. C. et al. 1998, Rev. Mod. Phys., 70, 1265

Angulo, C., et al. 1999, Nucl. Phys. A, 656, 3

Bedin, L. R., Cassisi, S., Castelli, F., Piotto, G., Anderson, J., Salaris, M., Momany, Y., & Pietrinferni, A. 2005, MNRAS, 357, 1038

Bell, R. A. & Gustafsson, B. 1978, A&AS, 34, 229

Bell, R. A. & Gustafsson, B. 1989, MNRAS, 236, 653

Bessell, M. S. 1990, PASP, 102, 1181

Bessell, M. S., & Brett, J. M. 1988, PASP, 100, 1134

Bessell, M. S., Castelli, F., & Plez, B. 1998, A&A, 333, 231

Bjork, S. R. & Chaboyer, B. 2006, ApJ, 641, 1102

Boesgaard, A. M., & Friel, E. D. 1990, ApJ, 351, 467

Carney, B. W., Lee, J.-W., & Dodson, B. 2005, AJ, 129, 656

Carpenter, J. M. 2001, AJ, 121, 2851

Carraro, G., Villanova, S., Demarque, P., McSwain, M. V., Piotto, G., & Bedin, L. R. 2006, ApJ, 643, 1151

Cassisi, S., Salaris, M., Castelli, F., & Pietrinferni, A. 2004, ApJ, 616, 498

Castelli, F. 1999, A&A, 346, 564

Castelli, F., Gratton, R. G., & Kurucz, R. L. 1997, A&A, 318, 841

Castelli, F., & Kurucz, R. L. 2003, IAU Symp. 210, ed. N. Piskunov, W. W. Weiss, & D. F. Gray (San Francisco: ASP), A20

Chaboyer, B., Fenton, W. H., Nelan, J. E., Patnaude, D. J., & Simon, F. E. 2001, ApJ, 562, 521

Chaboyer, B., Greene, E. M., & Liebert, J. 1999, AJ, 117, 1360

Chaboyer, B. & Kim, Y.-C. 1995, ApJ, 454, 767

Clem, J. L., Vandenberg, D. A., Grundahl, F., & Bell, R. A. 2004, AJ, 127, 1227

Cohen, M., Wheaton, W. A., & Megeath, S. T. 2003, AJ, 126, 1090

Cordier, D., Pietrinferni, A., Cassisi, S., & Salaris, M. 2007, AJ, 133, 468

de Bruijne, J. H. J., Hoogerwerf, R., & de Zeeuw, P. T. 2001, A&A, 367, 111

Demarque, P., Woo, J.-H., Kim, Y.-C., & Yi, S. K. 2004, ApJS, 155, 667

Dotter, A., Chaboyer, B., Jevremović, Baron, E., Ferguson, J. W., Sarajedini, A., & Anderson, J. 2007, AJ, 134, 376

Ferguson, J. W., Alexander, D. R., Allard, F., Barman, T., Bodnarik, J. G., Hauschildt, P. H., Heffner-Wong, A., & Tamanai, A. 2005 ApJ, 623, 585

Girardi, L., Bressan, A., Bertelli, G., & Chiosi, C. 2000, A&AS, 141, 371

Girardi, L., Castelli, F., Bertelli, G., Nasi, E. 2007, A&A, 468, 657

Grevesse, N. & Sauval, A. J. 1998, Space Sci. Rev., 85, 161 (GS98)

Grocholski, A. J. & Sarajedini, A. 2003, MNRAS, 345, 1015

Haft, M., Raffelt, G., & Weiss, A. 1994, ApJ, 425, 222

Harris, W.E. 1996, AJ, 112, 1487

Hauschildt, P. H., Allard, F., & Baron, E. 1999a, ApJ, 512, 377

Hauschildt, P. H., Allard, F., Ferguson, J., Baron, E., & Alexander, D. 1999b, ApJ, 525, 871

Houdashelt, M. L., Bell, R. A., & Sweigart, A. V. 2000, AJ, 119, 1448

Hubbard, W. B. & Lampe, M. 1969, ApJS, 18, 297

Iglesias, C.A. & Rogers, F.J. 1996, ApJ, 464, 943

Imbriani, G. et al. 2004, A&A, 420, 625

Irwin, A. 2004, Technical Report (http://freeeos.sourceforge.net)

Johnson, H. L. 1965, ApJ, 141, 923

Kalirai, J. S., Ventura, P., Richer, H. B., Fahlman, G. G., Durrell, P. R., D'Antona, F., & Marconi, G. 2001, AJ, 122, 3239

Korn, A.J., Grundahl, F., Richard, O., Barklem, P.S., Mashonkina, L., Collet, R., Piskunov, N., & Gustafsson, B., 2006, The Messenger, 125, 6

Kunz, R., Fey, M., Jaeger, M., Mayer, A., & Hammer, J. W. 2002, ApJ, 567, 643

Lee, Y.-W., Demarque, P., & Zinn, R. 1990, ApJ, 350, 155

Lee, Y. S. et al. 2007, submitted to AJ(http://arxiv.org/abs/0710.5778)

Montgomery, K. A., Marschall, L. A., & Janes, K. A. 1993, AJ, 106, 181

Paulson, D. B., Sneden, C., & Cochran, W. D. 2003, AJ, 125, 3185 (PSC)

Peterson, R. C. & Greene, E. M. 1998, ApJ, 502, 39

Origlia, L., Valenti, E., Rich, R. M., & Ferraro, F. R. 2006, ApJ, 646, 499

Pietrinferni, A., Cassisi S., Salaris M. & Castelli F. 2004, ApJ, 612, 168

Pietrinferni, A., Cassisi, S., Salaris, M., & Castelli, F. 2006, ApJ, 642, 797

Pinsonneault, M. H., Terndrup, D. M., Hanson, R. B., Stauffer, J. R. 2004, ApJ, 600, 946

Richer, H. B., Dotter, A., Hurley, J., Anderson, J., King. I., Davis, S., Fahlman, G. G., Hansen, B. M. S., Kalirai, J., Paust, N., Rich, R. M., & Shara, M. M. 2007, AJaccepted; http://arxiv.org/0708.4030

Sarajedini, A., Bedin, L. R., Chaboyer, B., Dotter, A., Siegel, M., Anderson, J., Aparicio, A., King, I., Majewski, S., Marín-Franch, A., Piotto, G., Reid, I. N., & Rosenberg, A. 2007, AJ, 133, 1658

Schlegel, D. J., Finkbeiner, D. P., & Davis, M. 1998, ApJ, 500, 525

Siegel, M. H., Dotter, A., Majewski, S. R., Sarajedini, A., Chaboyer, B., Nidever, D. L., Anderson, J., Marín-Franch, A., Rosenberg, A., Bedin, L. R., Aparicio, A., King, I., Piotto, G., Reid, I. N. 2007, ApJ, 667, 57

Sirianni, M. et al. 2005, PASP, 117, 1049

Spergel, D. N., et al. 2003, ApJS, 148, 175

Stetson, P. B., Bruntt, H., & Grundahl, F. 2003, PASP, 115, 413

Taylor, B. J. 2007, AJ, 133, 370

Thoul, A. A., Bahcall, J. N., & Loeb, A. 1994, ApJ, 421, 828

Vandenberg, D. A. & Bell, R. A. 1985, ApJS, 58, 561

Vandenberg, D. A., Bergbusch, P. A., & Dowler, P. D. 2006, ApJS, 162, 375

Vandenberg, D. A. & Clem, J. L. 2003, AJ, 126, 778 (VC03)

Vandenberg, D. A., Edvardsson, B., Eriksson, K., & Gustafsson, B. 2007, http://arxiv.org/0708.1188

Vandenberg, D. A. & Stetson, P. B. 2004, PASP, 116, 997

Yi, S. K., Demarque, P., & Kim, Y.-C. 2004, Ap&SS, 291, 261

Yi, S. K., Kim, Y.-C., Demarque, P. 2003, ApJS, 144, 259

Table 6.   Comparison Clusters

ID	DM_V	E(B–V)	[Fe/H]	Approximate Age (Gyr)	Photometry	Reference(s)
M 37	11.55	0.27	0.09	0.5	B V J K_s	1,2
Hyades	$\cdots$	$\cdots$	0.13	0.65	B V I K_s	3,4
NGC 2420	12.1	0.05	–0.27	2	B V I K_s	1
M 67	9.65	0.04	0	4	B V I K_s	1,5,6
NGC 6791	13.35	0.1	0.4	9	B V I K_s	7,8,9

References.   — 1–GS03, 2–Kalirai et al. (2001), 3–de Bruijne et al. (2001), 4–Pinsonneault et al. (2004), 5–Montgomery et al. (1994), 6–taylor, 7–Carney et al. (2005), 8–Stetson et al. (2003),9–Chaboyer et al. (1999)